**Alim Ormeci and Yuri Grin**

Max-Planck Institut für Chemische Physik fester Stoffe,
Nöthnitzer Str. 40, 01187 Dresden, Germany

# COEXISTENCE OF IONIC AND COVALENT ATOMIC INTERACTIONS (BONDING INHOMOGENEITY) AND THERMOELECTRIC PROPERTIES OF INTERMETALLIC CLATHRATES

*The influence of atomic interactions on the thermoelectric behavior of the Ba - Ge-based ternary clathrate-I phases $Ba_8T_xGe_{46-x-y}\Upsilon_y$ (T – main group element or late transition metal) has been investigated by means of quantum chemical techniques. The atomic interactions changes with the substituting element T were studied in real space by employing the electron localizability approach. Essentially two-center bonds in the framework (Ge – Ge and Ge – T) and predominantly ionic bonds between the guest and framework atoms were found. However, for T = Ag, Cd, Pt and Au, additional two-center Ba - T interactions were discovered. The type-I clathrates with such interactions are reported to have very low lattice thermal conductivity, revealing an important role of atomic interactions in the limiting of the thermal transport.*

**Key words:** intermetallic clathrates, chemical bonding, lattice thermal conductivity, QTAIM, electron localizability approach

## Introduction

Inorganic clathrates are an important group of intermetallic cage compounds. After the first report on *Na – Si* based clathrates in 1965 [1], the research activity on inorganic clathrates has steadily increased. Although there are a number of different clathrate structure types, the type-I clathrate phases have attracted most attention due to their relatively simple preparation and variability of chemical composition [2, 3, 4]. In type-I clathrate crystal structure four-coordinated atoms constitute a three-dimensional (3D) host framework with large cages that can accommodate guest atoms. Type-I clathrates crystallize in a simple cubic lattice and have the ideal composition $G_8Fw_{46}$ with 8 guest (*G*) and 46 framework (*Fw*) atoms, Pearson symbol *cP*54. The guest atoms can typically be alkali metals (*Na, K, Rb, Cs*), alkaline earths (*Sr, Ba*) or *Eu*. The framework mainly consists of group 14 elements, *Si*, *Ge*, *Sn*, and allows substitutions by other main group p elements or by electronegative transition metals. This flexibility in framework substitutions (which may be accompanied by inserting two elements, *G* and *G'*, as guest atoms) provides invaluable opportunities to tune various physical properties.

Silicon-based clathrate-I phases drew attention when superconductivity was reported in $(Na, Ba)_xSi_{46}$ [5] and $Ba_{8-x}Si_{46}$ [6] with transition temperatures of 4 and 8 K, respectively. Germanium-based clathrate-I phases, on the other hand, have been studied mostly for their potential use in thermoelectric (TE) applications. In general, all clathrate structures with their 3D framework - guest atoms in large cages type of arrangements are promising candidates as thermoelectric materials. This can be understood by considering the requirements for efficient TE performance. The thermoelectric performance of a material is assessed by a dimensionless figure of merit, $ZT = S^2 \sigma T / \kappa$. Here, *S* is the

Seebeck coefficient or thermopower, σ is the electrical conductivity, κ the thermal conductivity and *T* is the absolute temperature. Thermal conductivity has mainly contributions from electrons, $\kappa_e$, and from the lattice, $\kappa_L$. The former is directly proportional to the electrical conductivity, as described to a good approximation in the low- and high-temperature region through the Wiedemann-Franz law. Since both thermopower and electrical conductivity depend on charge carrier concentration, all terms in the figure of merit expression but the lattice thermal conductivity are determined largely by the charge carrier concentration of the TE material. Hence, increasing *ZT* to high values can be achieved by optimizing the charge carrier concentration. In order to improve the TE performance further, however, the lattice thermal conductivity, $\kappa_L$, should be reduced as much as possible. Consequently, the challenge in TE materials research can be summarized as finding a material that has good electronic but poor thermal transport properties. G. Slack introduced the concept of phonon glass electron crystal (PGEC) to describe this challenge [7]. The PGEC concept relies on the approximation that electronic and thermal transport properties of a compound can be modified rather independently of each other. Such a decoupling may be achieved in cage compounds with separated framework and guest substructures, as in clathrates or filled skutterudites, for example [4, 8]. The covalently bonded frameworks in the clathrate compounds are very convenient for purposes of optimizing the electronic part through substitution, while the guest atoms in the cages can impede the heat transport by giving rise to avoided crossings (between the acoustical branches and the guest-atom derived flat optical modes), however the actual mechanism is still debated [9, 10, 11, 12], in particular after inelastic scattering experiments revealing no evidence for an interpretation in terms of an isolated oscillator and showing rather coherent modes of guest and host substructures [10, 13].

The type-I clathrates obtained by substitution in the binary $Ba_8Ge_{43}\Upsilon_3$ are among the most intensely investigated clathrate phases. *ZT* values larger than 1.0 were reported at high temperatures (≥ 900 K) for $Ba_8Ga_{16}Ge_{30}$ (single crystal) [14] and $Ba_8Ni_{0.31}Zn_{0.52}Ga_{13.06}Ge_{32.2}$ [15], while polycrystalline $Ba_8Au_{5.3}Ge_{40.7}$ attains a *ZT* value of 0.9 at 680 K [16]. So far various ternary clathrate-I phases with a general composition $Ba_8T_xGe_{46-x-y}\Upsilon_y$ (where Υ stands for vacancy and *T* for the third element) were studied both experimentally and computationally in order to find compounds suitable for further improvement: *T* = *Ni* [17, 18, 19], *Cu* [17, 20, 21, 22], *Zn* [23, 24, 25, 26, 27], *Rh* [28], *Pd* [17, 29], *Ag* [17, 30], *Cd* [27, 31, 32], *Ir* [33], *Pt* [17, 34] and *Au* [16, 17, 35] as well as *Al* [36] and *Ga* [37, 38]. The homogeneity ranges vary greatly with the substituting element *T*, up to $x \approx 16$ for *Ga* [37], $x \approx 4.2$ for *Ni* [18] and $x \approx 0.4$ for *Ir* [33]. The binary clathrate-I phase in the *Ba* – *Ge* system ($x = 0$) has the composition $Ba_8Ge_{43}\Upsilon_3$ with three framework vacancies [39, 40]. The framework vacancies ($y \neq 0$) are also observed in ternary phases for small values of *x*. This large variation in chemical composition and the substituting elements give rise to a rich spectrum of physical properties. Electrical conductivity can be metallic or semiconducting; transitions from *n*- to *p*-type conduction are reported for the phases with *T* = *Ni* [19] and *Au* [16]; relatively low lattice thermal conductivities were observed for *T* = *Cu*, *Ag*, *Cd*, *Pt* and *Au*. Consequently, understanding the nature of this observed richness in respect of atomic interactions (chemical bonding) is of current interest.

The Zintl – Klemm concept is very useful in understanding the general features of the atomic interactions in clathrates. According to this concept the electropositive elements occupying the guest positions transfer their valence electrons to the framework so that the guest-framework interactions are mainly of ionic nature, and in the framework essentially two center-two electron ($2c – 2e$) covalent bonds are formed. In the case of complete electron balance, the number of available electrons matching the required number for all 92 ($2c – 2e$) framework bonds, a semiconducting behavior is expected. The case of excess electrons (electron deficiency) leads to *n*-type (*p*-type) electrical

conductivity. However, the discovery of covalent interactions between the guest atoms and some of the substitutions (see, for example, reference [16] for $Ba \leftarrow Au$ dative bonds) clearly indicates that quantum mechanics-based analytic tools are needed for a deeper understanding.

The atomic interactions in crystalline solids are usually studied by using quantities expressed in the reciprocal space, such as electron energy dispersions (bands and/or fat bands) and the electronic density of states (DOS). Recently this type of analysis is augmented by a real or direct space analysis, as well [41]. The electron localizability approach allows study of chemical bonding in real space using first-principles quantum mechanical calculations. This concept is in particular successful for intermetallic compounds. The real space analysis based on the electron localizability indicator (ELI [42]) resolves the shell structures of free atoms. Hence, when applied to a molecule or solid the core and valence regions are separated. The core electrons that do not participate in chemical bonding show spherically symmetric ELI distribution. The atomic interactions mostly take place in the valence region, and consequently the ELI distribution in this region is highly structured implying two- or multi-center bonds, or lone-pair-like features. In cases involving transition metal atoms a frequently encountered situation is the participation of the penultimate-shell electrons in chemical bonding which is manifested in the deviation of the ELI distribution in the penultimate shell from spherical symmetry [43, 49].

The electron localizability approach employs the topological analysis methods that play a central role also in the quantum theory of atoms in molecules (QTAIM) [44]. In QTAIM, the local maxima of the electron density usually occur at nuclear sites and the respective basins (QTAIM basins) are recognized as atoms in the crystal structure (molecule). The local ELI maxima, on the other hand, identify the inner electronic shells (core region) and the bonding interactions (valence region). Integrating the electron density inside the corresponding basins yields their electron populations. For the QTAIM or atomic basins the result will be the total number of electrons ($Q_A$) that an atom $A$ has in the given compound (molecule). For the basins of the ELI, number of core electrons for each atom and/or the electron populations of each bonding basin will be obtained. Whether a bonding basin represents a two- or multi-centered, or lone-pair-like interaction, can be determined by applying the basin intersection technique [45]. In this technique the bonding basin is intersected with the atomic basins and the number of electrons contributed to the bond by each atom can be found by integrating the electron density in each intersection region. For obtaining a more general picture of the atomic interactions, it is sometimes reasonable to ignore contributions less than some small fraction (e.g., 10%) of the bond population [46]. Furthermore, the basin intersection technique enables us to quantify bond polarity and explore its relation to electronegativity differences [47, 48]. Another useful feature of the ELI formulation is the possibility of decomposing it into partial contributions [49]. Partial ELI, denoted as pELI, can be obtained in terms of either energy windows (crystalline solids) or molecular orbital contributions (molecules).

In this study we investigate the chemical bonding in ternary clathrate-I compounds $Ba_8T_6Ge_{40}$ by combining the topological analysis of the electron density (ED) and the ELI in its ELI-D representation. The features of electronic DOS are used for discussion.

## Crystal Structure

The type-I clathrate structure consists of three framework and two guest atom positions (Fig. 1). These Wyckoff positions are 6*c*, 16*i*, 24*k* and 2*a*, 6*d*, respectively, in the space group $Pm-3n$ (no. 223). Only the 16*i* ($x\ x\ x$) and 24*k* ($0\ y\ z$) positions have free parameters, others' coordinates are fixed by symmetry. In the context of $Ba_8T_6Ge_{40}$ clathrate phases the framework positions can be labeled as 6*c* = *Ge*1, 16*i* = *Ge*2 and 24*k* = *Ge*3. The *Ge*2 and *Ge*3 sites form two 20 – atom cages per unit cell,

while all framework atoms participate to form six 24 – atom cages per unit cell. The former are centered by the guest atoms at 2*a* and the latter at 6*d* positions. Each framework atom is four-coordinated by other framework atoms. This structural feature yields 24 × *Ge*1 – *Ge*3, 8 × *Ge*2 – Ge2, 12 × *Ge*3 – *Ge*3 and 48 × *Ge*2 – *Ge*3 contacts per formula unit. Hence, in total the framework contains 92 two-center two-electron bonds requiring 184 valence electrons per unit cell. The diamond structure is also generated by four-coordinated atoms, however the less dense clathrate-I framework differs from it significantly by the presence of three planar hexagons per unit cell. These hexagons are formed by two *Ge*1 and four *Ge*3 atoms. In the plane of the hexagons the *Ge*3 – *Ge*3 – *Ge*1 angles usually vary around 125 degrees deviating strongly from the tetrahedral value of 109.47 degrees. In addition, the hexagons along a crystallographic axis alternate between being "horizontal" and "vertical" so that two neighboring hexagons meet at the common *Ge*1 (6*c*) sites. Therefore, these sites are expected to behave differently in comparison to the other two framework sites. In fact, point defects, especially at relatively low concentrations, are observed to involve mostly the 6*c* Wyckoff position. In particular, in the binary clathrate-I compound $Ba_8Ge_{43}\square_3$ only half of the 6*c* sites are occupied by the *Ge* atoms [39]. The vacancies can be taken, to a good approximation, as fully ordered so that a 2 × 2 × 2 supercell in space group *Ia* – 3*d* (no. 230) with Pearson symbol *cI408* results [39, 40].

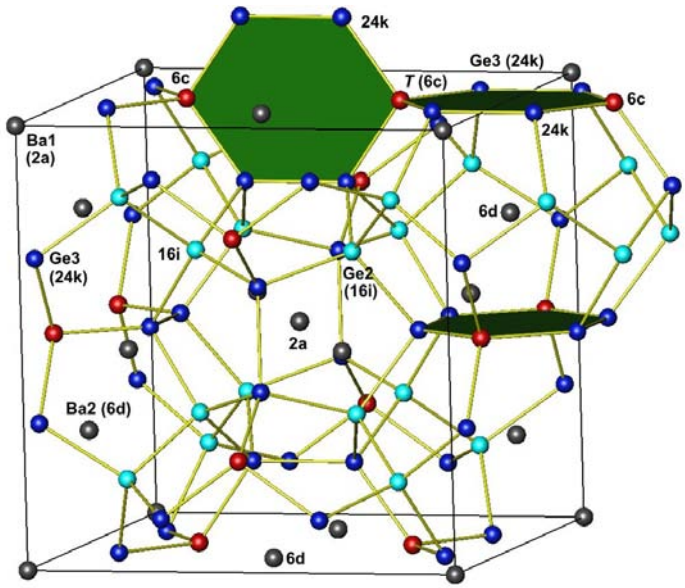


*Figure 1. Crystal structure of clathrate-I* $Ba_8T_6Ge_{40}$.

In the ternary clathrate-I compounds $Ba_8T_xGe_{46-x-y}\square_y$, the *T* atoms are usually located at the 6*c* sites for $x < 6$. Moreover, the vacancies are found exclusively at the 6*c* sites (reminiscent of the binary clathrate $Ba_8Ge_{43}\square_3$). Consequently, almost all $Ba_8T_xGe_{46-x-y}\square_y$ phases are structurally disordered resulting in complex crystal structures. However, the main purpose of this study is to investigate chemical bonding in ternary type-I clathrate compounds in real space with emphasis on *Ba* – *T* and *T* – *Ge* interactions and the effects of these interactions on the *Ge* – *Ge* bonds. The complications due to the crystal structure were avoided by employing a simplified structural model with all 6*c* sites occupied by *T* atoms. The corresponding fully-ordered crystal structure model has the composition $Ba_8T_6Ge_{40}$. We consider the cases *T* = *Li*, *Mg*, *Al*, *Ga* and the late transition metals belonging to groups 9 – 12 of the Periodic Table. For comparison, the empty ($\square_8Ge_{46}$) and the binary ($Ba_8Ge_{43}\square_3$) clathrates as well as the hypothetical $Ba_8Ge_{46}$ were included in the study.

## Quantum chemical techniques

Electronic structure calculations were performed by using the all-electron, full-potential local orbital (FPLO) method [50] (version 9.01). All main results were obtained within the local density approximation (LDA) to the density functional theory through the Perdew-Wang parametrization for the exchange-correlation effects [51]. Some of the results were compared to those obtained by the generalized gradient approximation (GGA) [52] and no significant differences were found. In the FPLO method a scalar relativistic Hamiltonian is applied to the semi-core and valence electrons, while the core electrons are treated in a fully-relativistic way. Chemical bonding analysis is based on the combined analysis of electron density (ED) and electron localizability indicator (ELI). ELI [42] was calculated in the ELI-D representation [53, 54] by a module implemented into FPLO software [55]. Topological analysis of the ED and the ELI-D were carried out by the program DGrid [56].

The crystal structures of the type-I clathrates $\Upsilon_8Ge_{46}$, $Ba_8Ge_{46}$ and $Ba_8T_6Ge_{40}$ were fully optimized within LDA using a Brillioun zone (BZ) mesh of 8 × 8 × 8 and placing all *T* atoms at the 6*c* Wyckoff position of the space group $Pm-3n$ (no. 223). The maximum orbital angular momentum number was set to 12 for electron density expansion. The maximum force criterion was 5 meV $Å^{-1}$ and the equilibrium volume determination process was stopped when the estimated change in the lattice parameter was less than ~ 0.004 Å (corresponds to a volume ratio of ~0.1 %). For $Ba_8Ge_{43}\Upsilon_3$ the vacancy-ordered 2 × 2 × 2 superstructure model [39] was used without atomic position or unit cell volume optimization. The ELI-D and DOS calculations at the minimum-energy structures utilized a BZ mesh of 10 × 10 × 10.

## Results and Discussion

The optimized values of the crystal structure parameters for $Ba_8Ge_{46}$ and $Ba_8T_6Ge_{40}$ where *T* = *Li*, *Mg*, *Al*, *Ga* and transition metals of groups 9 – 12 are listed in Table I.

*Table 1.*

Optimized lattice parameters and atomic coordinates of *Ge*2 (16*i* site) and *Ge*3 (24*k* site) in the model $Ba_8T_6Ge_{40}$ structures.

| Composition | *a* (Å) | *x* (16*i*) | *y* (24*k*) | *z* (24*k*) |
|---|---|---|---|---|
| $Ba_8Li_6Ge_{40}$ | 10.7126 | 0.1827 | 0.3118 | 0.1153 |
| $Ba_8Mg_6Ge_{40}$ | 10.8433 | 0.1836 | 0.3040 | 0.1139 |
| $Ba_8Al_6Ge_{40}$ | 10.7602 | 0.1843 | 0.3086 | 0.1184 |
| $Ba_8Ga_6Ge_{40}$ | 10.7612 | 0.1845 | 0.3092 | 0.1186 |
| $Ba_8Ge_6Ge_{40}$ | 10.8964 | 0.1847 | 0.3074 | 0.1183 |
| $Ba_8Co_6Ge_{40}$ | 10.5064 | 0.1829 | 0.3255 | 0.1263 |
| $Ba_8Ni_6Ge_{40}$ | 10.5098 | 0.1829 | 0.3233 | 0.1245 |
| $Ba_8Cu_6Ge_{40}$ | 10.5643 | 0.1830 | 0.3180 | 0.1198 |
| $Ba_8Zn_6Ge_{40}$ | 10.6500 | 0.1837 | 0.3118 | 0.1183 |
| $Ba_8Rh_6Ge_{40}$ | 10.6380 | 0.1831 | 0.3185 | 0.1216 |
| $Ba_8Pd_6Ge_{40}$ | 10.6624 | 0.1830 | 0.3146 | 0.1187 |
| $Ba_8Ag_6Ge_{40}$ | 10.7484 | 0.1830 | 0.3085 | 0.1157 |
| $Ba_8Cd_6Ge_{40}$ | 10.8410 | 0.1838 | 0.3028 | 0.1149 |
| $Ba_8Ir_6Ge_{40}$ | 10.6539 | 0.1832 | 0.3178 | 0.1219 |
| $Ba_8Pt_6Ge_{40}$ | 10.6631 | 0.1831 | 0.3148 | 0.1202 |
| $Ba_8Au_6Ge_{40}$ | 10.7238 | 0.1832 | 0.3093 | 0.1169 |
| $Ba_8Hg_6Ge_{40}$ | 10.8454 | 0.1837 | 0.3024 | 0.1155 |

**Electronic structure**

Since, each framework atom is four-coordinated by other framework atoms in an approximately tetrahedral environment, an empty clathrate such as $\Upsilon_8Ge_{46}$, in analogy to the diamond structure, is expected to have an energy band gap [57]. Indeed, we obtained a band gap of 1.22 eV for the fully-optimized $\Upsilon_8Ge_{46}$ structure. The corresponding electronic density of states (DOS) is presented in Figure 2, upper panel. In $Ba_8Ge_{43}\Upsilon_3$, there are 16 extra electrons from the *Ba* atoms, but due to the missing three *Ge* atoms at the 6*c* position the net number of the excess electrons is four: $(Ba^{2+})_8[(3b)Ge^-]_{12}[(4b)Ge^0]_{31}\cdot 4e^-$, where (*3b*) and (*4b*) denote three- and four-bonded *Ge*, respectively. The calculated electronic structure of $Ba_8Ge_{43}\Upsilon_3$ [58] shows that the band gap of $\Upsilon_8Ge_{46}$ is preserved although its width is reduced to about 0.2 eV, and top of the gap lies 0.5 eV below the Fermi energy ($E_F$, Fig. 2, middle panel). The number of electrons occupying the states between -0.5 eV and Fermi energy (set to 0 eV) is exactly four, in agreement with the above simple electron counting. For the hypothetical binary clathrate-I $Ba_8Ge_{46}$ the net number of the excess electrons is 16 and therefore top of the gap lies further below the $E_F$, at about -0.85 eV (Fig. 2, lower panel). The width of the gap is ~0.6 eV. The preservation of the gap implies that the *Ba* states, mainly *5d*, hybridize only weakly with those of the *Ge* framework in the region below the gap.

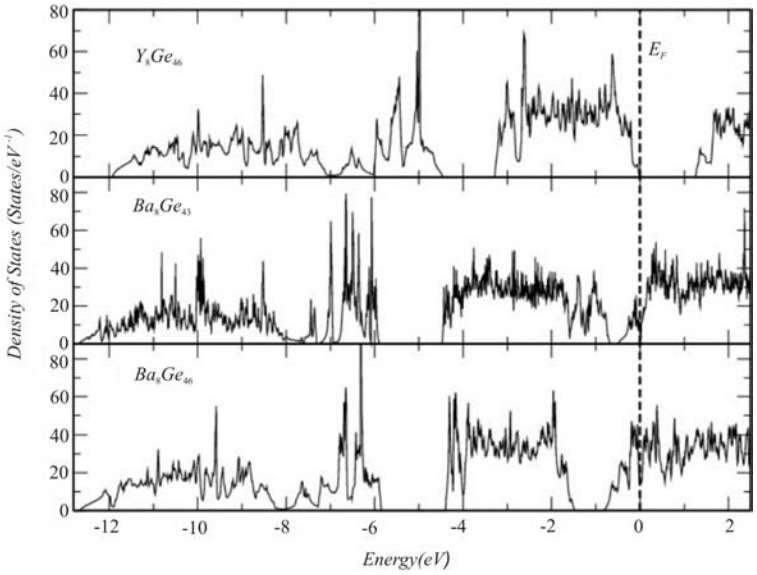


*Fig. 2. Calculated electronic density of states for $\Upsilon_8Ge_{46}$, $Ba_8Ge_{43}\Upsilon_3$, and $Ba_8Ge_{46}$.*

An important question is what happens to the gap when atoms of a third element are introduced to the clathrate-I structure. In the case of *Ba – T – Si* type-I clathrate phases for *T = Ni* [59] and *Rh* [60], the rather strong hybridization between the *d* electrons of *T* and the *p* electrons of Si results in the closing of the gap (reminiscent of the empty $\Upsilon_8Si_{46}$ clathrate). In contrast, we find for the case of $Ba_8T_6Ge_{40}$, that the band gap persists even when six atoms of the element *T = Li, Mg, Al, Ga* (Fig. 3) or a transition metal from groups 9 through 12 (Fig. 4) replace the *Ge* atoms at the *6c* position. The Fermi energy lies above or below the gap depending on the ability of the *T* elements to a accommodate valence electrons of *Ba* with respect to the empty clathrate $\Upsilon_8Ge_{46}$. According to the Zintl-Klemm concept each *T* atom would need four electrons for forming four two-electron two-center bonds with the neighboring *Ge* atoms. The difference between four and the number of valence electrons *v* of the *T* atom yields its accommodation ability of *T*. The comparison of the accommodation ability of six *T* atoms with the 16 electrons transferred from *Ba* determines the location of the gap with respect to $E_F$:

if the accommodation ability of six *T* is less than 16, the gap is below the Fermi level and *vice versa*. The DOS results to be presented below show the validity of this argumentation providing support for the applicability of the Zintl-Klemm concept to the ternary clathrate-I phases $Ba_8T_6Ge_{40}$.

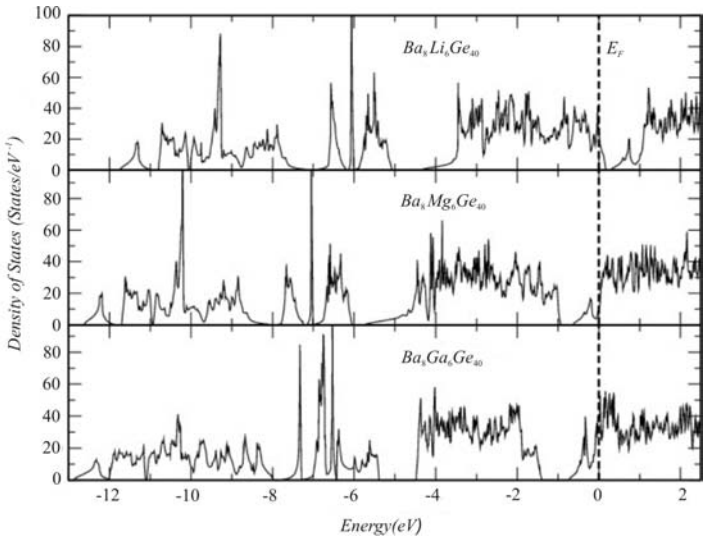


*Fig. 3. Calculated electronic density of states for $Ba_8T_6Ge_{40}$ with T = Li, Mg, Ga.*

Lithium has one valence electron, therefore in $Ba_8Li_6Ge_{40}$ there are two electrons less compared to $\Upsilon_8Ge_{46}$: $(Ba^{2+})_8[(LiGe_4)^{3-}]_6[(4b)Ge^0]_{16}\cdot 2e^+$, where $e^+$ stands for a hole. Hence, the gap is above $E_F$ (Fig. 3 upper panel) and the integrated DOS between $E_F$ and bottom of the gap reveals two electrons as expected. Similar count for *Mg* and *Ga* (two and three valence electrons, respectively) yields 4 and 10 extra electrons – $(Ba^{2+})_8[(MgGe_4)^{2-}]_6[(4b)Ge^0]_{16}\cdot 4e^-$ and $(Ba^{2+})_8[(GaGe_4)^{1-}]_6[(4b)Ge^0]_{16}\cdot 10e^-$, respectively – so that $E_F$ ends up above the gap (Fig. 3 middle and lower panels). In these cases also the integrated DOS between top of the gap and $E_F$ gives the expected electron numbers.

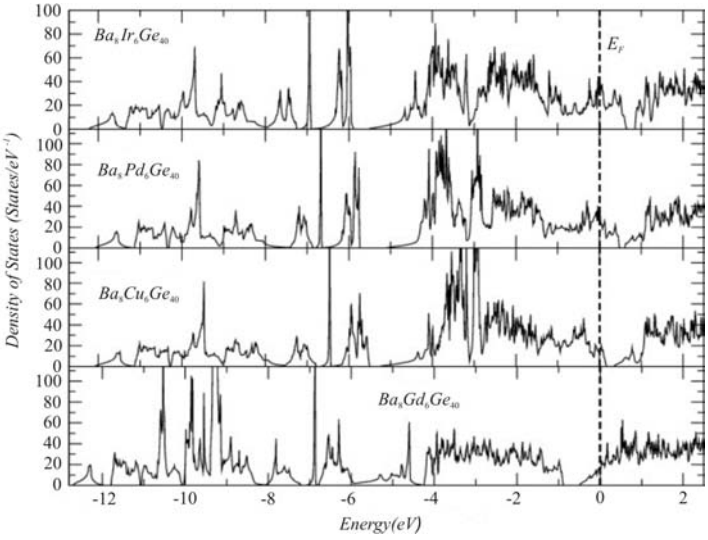


*Fig. 4. Calculated electronic density of states for $Ba_8T_6Ge_{40}$ with T = Ir, Pd, Cu and Cd.*

By comparing Figs. 3 and 4, we deduce similar behavior for *T = Li, Cu, Ag, Au* and for *T = Mg, Zn, Cd, Hg* sets showing DOS consistent with the picture for *T* having one or two valence electron(s). Recent experimental and theoretical work on $Ba_8Au_xSi_{46-x}$ [61] and $Ba_8Au_xGe_{46-x}$ [16] phases have revealed that as *x* is varied from below 5.33 to above 5.33 the nature of the charge carrier transport in the corresponding compounds changes from *n*-type (electron-rich case) to *p*-type (electron-poor case).

This transition can be explained if *Au* atoms act as having one valence electron so that each of them needs three electrons from the *Ba* atoms to make two-electron bonds with *Ge* neighbors. The critical value of $x = 16/3 = 5.33$ to match the number of available electrons to the electron demand is simply the number of *Au* atoms that can accommodate all 16 electrons available from *Ba*. Group 10 elements have one electron less than their group 11 neighbors, thus they are expected to behave as if they have zero valence electrons. With ν set to 0 we obtain accommodation ability of 24 for 6 *Pd* atoms. With 16 available electrons of 8 *Ba* species, it places the $E_F$ below the gap. The computed DOS (Fig. 4, *T* = *Pd*) is in agreement with this expectation, and the integrated DOS from $E_F$ to the bottom of the gap yields 8 electrons as expected. The electron balance for *T* = *Ni* can be – similarly to the *Pd* case - expressed as $(Ba^{2+})_8[(NiGe_4)^{4-}]_6[(4b)Ge^0]_{16}\cdot 8e^+$. Experimental evidence for the electronic state of *Ni* exists for $Ba_8Ni_xGe_{46-x-y}\Upsilon_y$ [19] and $Ba_8Ni_xSi_{46-x-y}\Upsilon_y$ phases [63], for which X-ray absorption studies carried out on *Ni* sites suggest an oxidation state close to that of elemental *Ni*. In the case of group 9 elements, one electron less than in group 10, one would set ν to -1, e.g., $(Ba^{2+})_8[(CoGe_4)^{5-}]_6[(4b)Ge^0]_{16}\cdot 14e^+$, so that $E_F$ falls further below the gap (Fig. 4, top panel). For all group 9 elements the states between $E_F$ and the bottom of the gap are found to accommodate 14 electrons.

The electron balances derived from the Zintl model of atomic interactions in clathrates and their correlation with the electronic density of states allow description of the electronic transport in this family of thermoelectric materials for any values of *x* within the experimentally found homogeneity ranges of the phases $Ba_8T_xGe_{46-x-y}\Upsilon_y$. Analysis of the thermal transport behavior reveals that the lattice thermal conductivity does not follow the changes in the electronic structure [10] and shows for the case of *T* = *Au* some influence of the distinct atomic interactions in the crystal structure [16]. A systematic analysis of such interactions is made by real-space quantum chemical techniques.

**Chemical bonding in real space**

The QTAIM basins and their electron populations were obtained for the $Ba_8T_6Ge_{40}$ clathrates by applying the topological analysis to the electron density. The shapes of QTAIM basins are shown in Fig. 5 for $Ba_8Cu_6Ge_{40}$. One notices that both *Ba*1 and *Ba*2 basins have highly spherical shapes. This implies that *Ba* atoms act mainly as cations: the atomic basin of an ideal cation should consist only of the core electron shells whose electron density would have a spherical distribution. The QTAIM basins of the *Ge* and *Cu* atoms, on the other hand, are far from being spherical indicating the presence of more directional interactions (in comparison with the ionic ones).

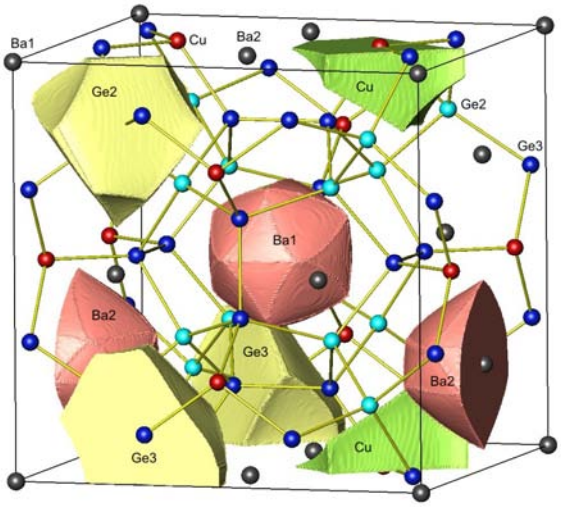


*Fig. 5. QTAIM atoms in $Ba_8T_6Ge_{40}$ by the example of T = Cu.*

The effective charge of an atom within the electron localizability approach is defined as the difference between the atomic number $Z$ and the electron population of the atomic basin $Q$. Fig. 6 shows the calculated effective charges ($Z - Q$) of the $T$ atoms in relation to their position in the Periodic Table. Due to the similarity of the electronic DOS, *Li* and *Mg* are assigned to groups 11 and 12, respectively, for plotting purposes. Large positive effective charges are observed for the main group elements *Li*, *Mg* and *Al*. Normalizing the effective charges for one formal valence one obtains +0.80, +0.65 and +0.47, respectively, correctly reproducing the order of increasing electronegativity (*EN*) within one row. The main group element of the next row – gallium – has a smaller positive effective charge than aluminum being also in agreement with the electronegativity of the elements of group 13 (*EN*(*Ga*) > *EN*(*Al*). There are two general remarks in regard to the transition metals: the effective charges (i) get more negative within each group as period number increases, (ii) get less negative within each period as group number increases. Both observations are in line with the general tendency of how electronegativity changes across the Periodic Table. *Ge*3 atoms are the nearest neighbors of the *T* ones; therefore their effective charges vary in a wide range. One limit corresponds to the case of electropositive elements $(Z - Q)_{Ge3} \approx -0.60$ for *T* = *Mg* and *Al*, and the other to *Ir* and *Pt* with $(Z - Q)_{Ge3} \approx -0.05$. *Ba*2 and *Ge*2 effective charges show a variation of approximately the same width: (1.2 ÷ 1.4) for *Ba*2 and (-0.3 ÷ -0.1) for *Ge*2. Since the *Ba*1 – *T* and *Ba* – *Ge* distances (> 0.559 times the lattice parameter) are the longest among the host-guest distances, *Ba*1 effective charges change very little, they lie between 1.1 and 1.2.

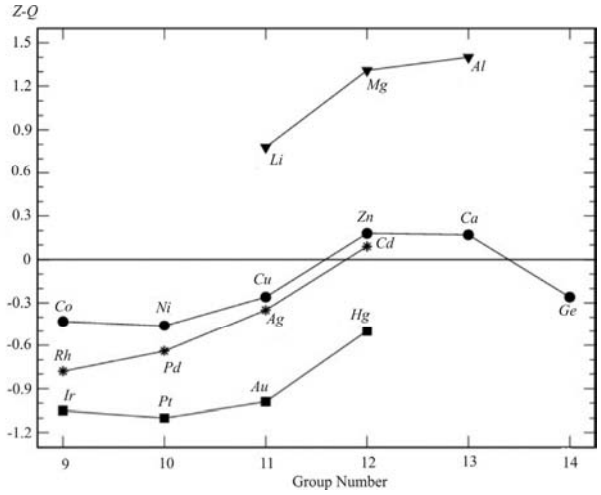


*Fig. 6. Effective charges for QTAIM atoms in $Ba_8T_6Ge_{40}$.*

More insight about how *Ge* – *T* and *Ge* – *Ge* interactions are affected as *T* is changed was gained by performing the topological analysis of the ELI-D. The ELI-D distributions at $x = a/2$ for some representative cases are shown in Figure 7. Apart from the *Ge*2 – *Ge*2 and *Ge*2 – *Ge*3 bonds all other bonding situations of interest are present in this plane. The *Ge*3 – *Ge*3 attractors are off the bond line, but usually very close to it. Electron populations of bond basins are calculated by integrating the ED inside the valence-region ELI-D basins. Basin intersection technique is used to determine how many electrons are contributed by which atoms. In general the *Ge* – *Ge* bonds have a two-center character with *Ba* contributions always being less than ~ 2% of the bond population. In the empty clathrate $\Upsilon_8Ge_{46}$ there are, as expected, only two-center two-electron *Ge* – *Ge* bonds. In $Ba_8Ge_{43}$, due to the vacancies at the 6*c* site, the basins of the former *Ge*1 – *Ge*3 bonds have contact only to one *Ge*3 core, i.e., they represent lone pairs at *Ge*3 atoms [64]. The bond populations are as follows: for *Ge*2 – *Ge*2 bond – 2.25 $e^-$, for *Ge*3 – *Ge*3 bond – 1.95 $e^-$, for *Ge*1 – *Ge*3 bond – 2.17 $e^-$, for *Ge*3 lone pair – 2.52 $e^-$

and for *Ge*2 – *Ge*3 bond – 2.10 $e^-$ (when *Ge*3 has a *Ge*1 neighbor), 1.92 $e^-$ (for *Ge*2 at 32*e* position) and 2.05 $e^-$ (when *Ge*2 is at 96*h* position and *Ge*3 has a lone pair). These values are essentially independent of whether LDA or GGA is used in the calculation.

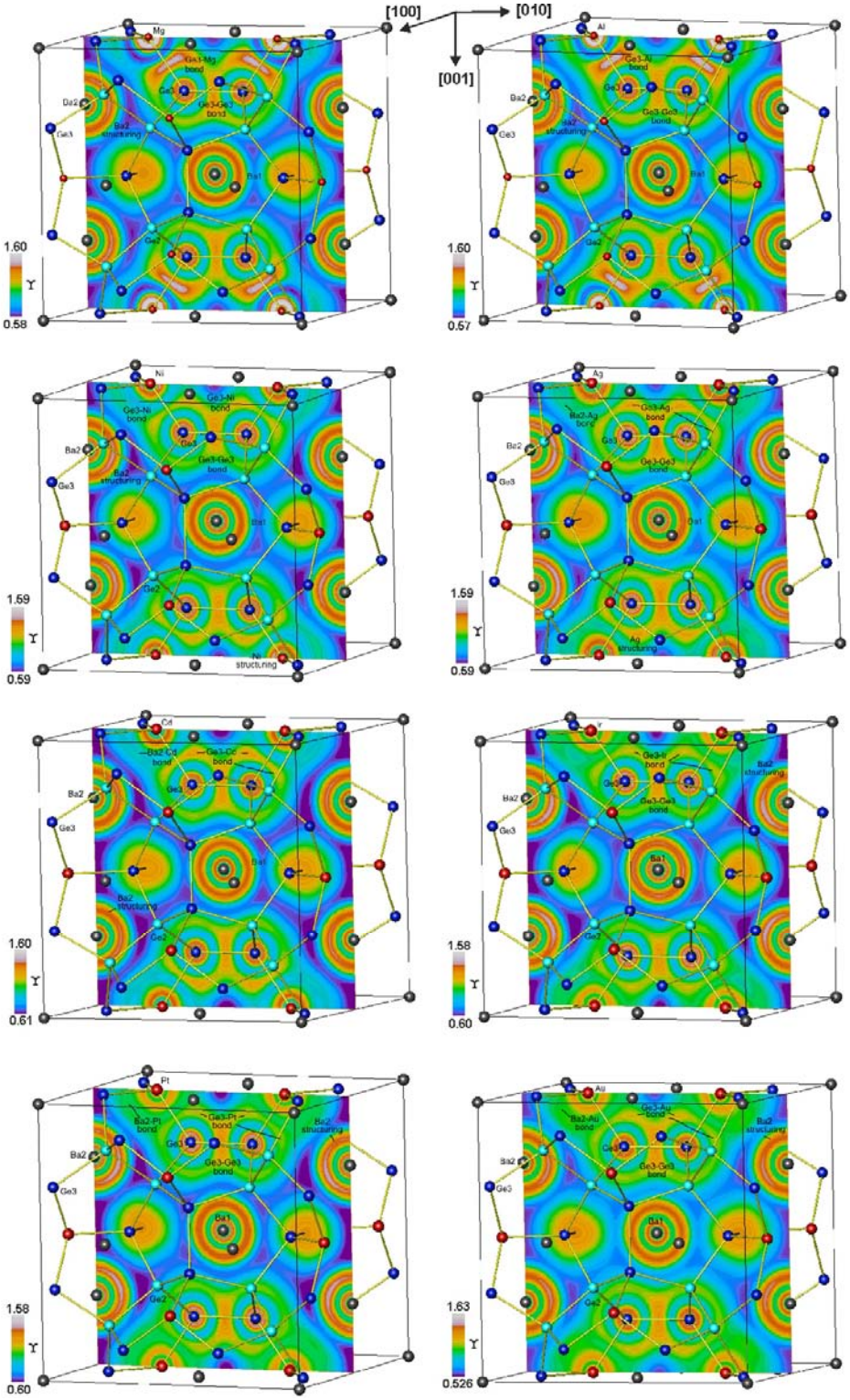


*Fig. 7. ELI-D distribution in $Ba_8T_6Ge_{40}$ at x = 0.5 for T = Mg, Al, Ni, Ag, Cd, Ir, Pt, Au.*

The *Ge* – *Ge* bond populations are plotted against *Ge* – *Ge* distances in the studied $Ba_8T_6Ge_{40}$ clathrates in Fig. 8. The *Ge*2 – *Ge*2 bonds are the least affected by *T* due to the rather long *Ge*2 – *T*

contacts of about 4 Å. Their bond populations vary between 2.2 and 2.3 electrons and the *Ge*2 – *Ge*2 distances lie between 2.44 and 2.50 Å. The *Ge*2 – *Ge*3 distances vary in a narrow range, 2.48 – 2.53 Å, but the bond populations show a wider variation: 1.88 to 2.15 electrons. As expected, the *Ge*3 – *Ge*3 values are spread over considerably wider ranges of [1.7, 2.05] $e^-$ and [2.47, 2.66] Å for bond population and bond distance, respectively. In the *Ge*2 – *Ge*2 and *Ge*3 – *Ge*3 bonds, *Ge* atom contributions are equal, but the *Ge*2 – *Ge*3 bonds are slightly polar (similar to the *Ge*3 – *Ge*1 case above) due to different local environments [66].

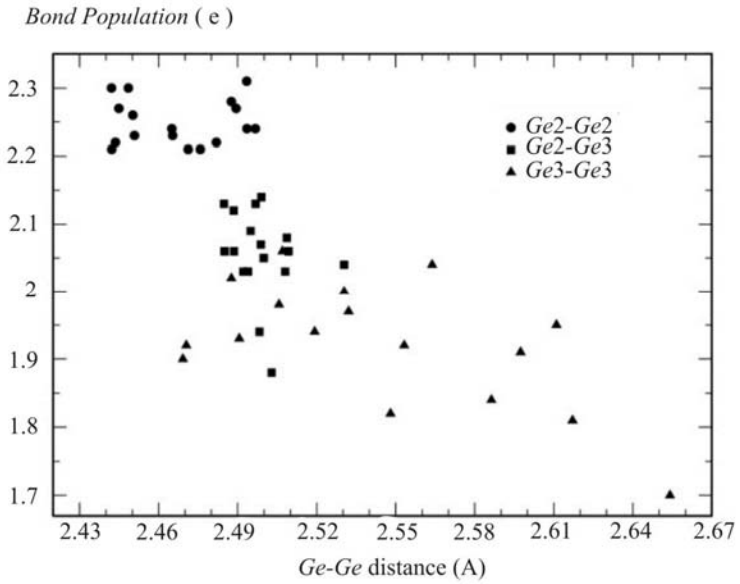


*Fig. 8. Ge - Ge bond populations versus Ge - Ge bond distances in $Ba_8T_6Ge_{40}$.*

The *Ge*3 – *T* bond attractors have in the isolated *GeT* molecules usually ring characteristics [43, 49]. In the $Ba_8T_6Ge_{40}$ clathrates, due to the non-cylindrical symmetry of the *Ge* – *T* bond environment they are split into two for all transition metals (Fig. 7). In addition, the structuring of the penultimate shell is observed for most transition metals, e.g. for the 3rd and 4th shells for *Ni* and *Ag*, respectively, it is noted in Fig. 7. The structuring of the penultimate shell of the *T* species is very weak for group 12 atoms and is missed in the case of main group elements. The bond polarity of the *Ge* – *T* bonds is a consequence of the different atomic charges of the participating atoms.

Information on *Ba* – framework interactions can be inferred from the structuring of *Ba* atoms' penultimate (5th) shell. In all cases the structuring of *Ba*2 penultimate shell is significant enough to be noticed in two-dimensional plots of the ELI-D distribution (Fig. 7). In contrast, *Ba*1 structuring is comparatively very small, it is noticeable only for *T* = *Pt*. In the ELI-D representation of the *Ba* atom, the 5*p* states contribute also to the valence region. i.e., they may as well be participating in atomic interactions. An interesting finding is the detection of two-center *Ba*2 ← *T* dative bonds for *T* = *Ag*, *Cd*, *Pt* and *Au* manifested by the dedicated ELI-D attractor (Fig. 7). Covalent *Ba*2 – *Au* bonds were reported in a previous study which employed the tight-binding linear-muffin-tin orbital (TB-LMTO) method [16]. This result is confirmed in the present FPLO calculations by applying either LDA or GGA techniques. Additionally, three new cases are found. Bond populations are 0.10, 0.06, 0.16 and 0.27 electrons for *Ag*, *Cd*, *Pt* and *Au*, respectively. These bonds are strongly polar with the bond fraction [48] of *Ba*2 atoms being 0.05 – 0.06. Because some of the *Pt* or *Au* electrons are used for forming the according dative *Ba*2 – *T* bonds, the low values of bond populations of the *Ge*3 – *Pt* and *Ge*3 – *Au* bonds are partly understandable. The partial ELI-D analysis based on the energy window

decomposition confirms the *T*(*d*) participation for *T* = *Ag*, *Pt* and *Au*. Here, the *Ba*2 – *T* ELI-D attractors show up when the lower limit of the energy window is chosen above the energy ranges dominated by the *T*(*d*) states. The upper limit is taken as the Fermi energy. The lower limits for the chosen energy windows are -4.15, -2.88 and -3.95 eV for *Ag*, *Pt* and *Au*, respectively. In these energy ranges *Ba* 5*d* contributions start to rise and transition metal *d* contribution remain below 10 states $eV^{-1}$. However, for *T* = *Cd* similar analysis failed to isolate an energy window where *Ba*2 – *Cd* ELI-D bond attractors occur. Here, the *Ba* – *Cd* bonding attractor results from the contributions of the whole valence manifold of *Cd*.

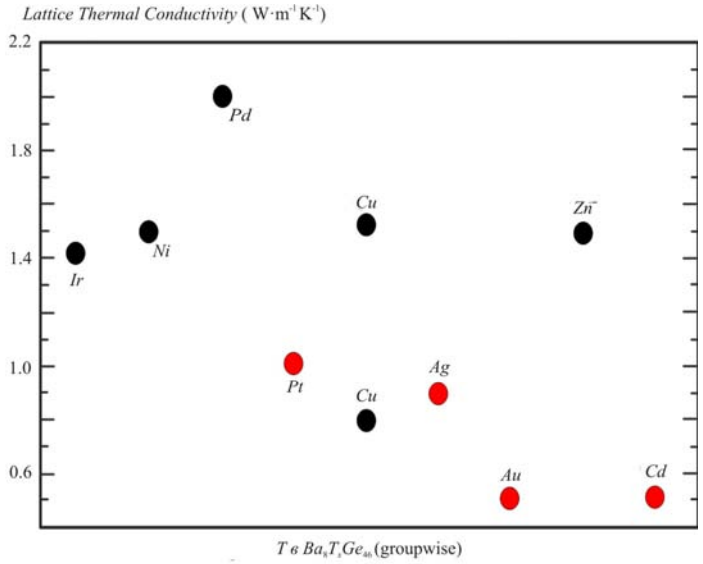


*Fig. 9. Experimental minimum lattice thermal conductivity values at temperatures above 200 K for the $Ba_8T_xGe_{46-x}$ phases (100 K for T = Ir). Red points mark the T elements forming Ba – T bonds (cf. text).*

Analysis of the lattice thermal conductivity $\kappa_L$ of the ternary type-I clathrates $Ba_8T_xGe_{46-x-y}\Upsilon_y$ reported in the literature reveals strongly reduced values for all compounds having *Ba*2 – *T* bonds (Fig. 9). The $\kappa_L$ is around 0.9 and 1.0 W $m^{-1}$ $K^{-1}$ for *Ag* and *Pt* [30, 34], respectively; it varies between 0.5 – 1.5 and 0.5 – 1.0 W $m^{-1}$ $K^{-1}$ for *Cd* and *Au* [16, 31, 65], respectively. As a comparison, $\kappa_L$ values are above 1.4 – 1.5 W $m^{-1}$ $K^{-1}$ for *Ir* [66], *Ni* [18, 19] and *Zn* [23], and above 2.0 W $m^{-1}$ $K^{-1}$ for *Pd* [29]. Moreover, the $\kappa_L$ values for the $Rb_{7.88}Au_{2.47}Ge_{43.53}$ clathrate are higher than 1.5 W $m^{-1}$ $K^{-1}$, and the ELI-D analysis on $Rb_8Au_6Ge_{40}$ found no dedicated maxima on the *Rb* – *Au* contacts [67]. The exceptional case is that of *T* = Cu: the minimum value of $\kappa_L$ is reported to be around 0.8 W $m^{-1}$ $K^{-1}$ [68], but the ELI-D analysis finds no *Ba*2 – *Cu* interaction with an dedicated attractor. Usually the low lattice thermal conductivities obtained for heavier *T* elements are explained as a mass effect, however the systematic investigation of the $Ba_8Au_xGe_{46-x}$ clathrate in very narrow range of $5.25 \le x \le 5.50$ revealed the change of $\kappa_l$ from 0.55 to 0.9 W $m^{-1}$ $K^{-1}$ confirming rather the role of the *Ba* – *Au* bonding [65]. Furthermore, the iridium-containing clathrate with heavy *T* component does not show reduced lattice thermal conductivity, being in agreement with the absence of *Ba* – *Ir* interaction [66]. However, a role of the covalent *Ba*2 – *T* interactions deserves further investigation. In particular, further experimental work on *Hg* – and *Cu* – containing clathrates will be illuminating, because mercury is heavy and no *Ba*2 – *T* bonds were detected in the ELI-D analysis, and the *vice versa* case represents *T* = *Cu*, whereby the experimental data differ quite strongly from 0.8 to 1.5 W $m^{-1}$ $K^{-1}$ [21, 68] (Fig. 9).

## Summary

The chemical bonding in ternary *Ba – Ge* - based clathrate-I phases is investigated by applying the QTAIM and electron localizability approach. The composition $Ba_8T_6Ge_{40}$ is used for the quantum chemical calculations where *T* atoms occupy the 6*c* Wyckoff position. The QTAIM analysis of the electron density shows that *Ba* atoms transfer about 1.2 – 1.3 electrons to the $[T_6Ge_{40}]$ framework. The *Ge*2 atoms coordinated only by germanium receive 0.1 – 0.2 electrons. The *Ge*3 atoms have *T* atoms in the first coordination sphere; thus, the effective charges of *Ge*3 vary more strongly from -0.05 to -0.60 depending on the polarity of the *Ge*3 – *T* bond. The *Ge – T* interactions are found to be essentially of two-center character with negligible *Ba*2 contributions. *Ba* – framework interactions are mostly ionic as expected from the Zintl-Klemm concept. However, the electrons in the 5$^{th}$ (penultimate) shell of *Ba* atoms do participate in atomic interactions with the framework atoms as judged from the non-spherical ELI-D distribution in these shells (structuring) and from the electronic DOS. Moreover, for *T = Cd, Ag, Pt* and *Au*, there are dedicated ELI-D bond attractors indicating two-center *Ba*2 – *T* interactions. Coexistence of different types of bonding in the clathrates $Ba_8T_6Ge_{40}$ is named as bonding inhomogeneity. The lattice thermal conductivity of the clathrate-I phases with these *Ba*2 – *T* bonds were reported to be lower in comparison with the phases without *Ba*2 – *T* bonding suggesting that such bonds play a role in heat transfer reduction.

## References

1. J.S. Kasper, P. Hagenmuller, M. Pouchard, and C. Cros, Clathrate Structure of Silicon $Na_8Si_{46}$ and $Na_xSi_{136}$ (x < 11), *Science* 150, 1713 – 1714 (1965).
2. M. Christensen, S. Johnsen, and B.B. Iversen, Thermoelectric Clathrates of Type I, *Dalton Trans*. 39, 978 – 992 (2010).
3. S. Stefanoski, M. Beekmann, and G.S. Nolas, Inorganic Clathrates for Thermoelectric Applications in *The Physics and Chemistry of Inorganic Clathrates*, ed. G. S. Nolas (Springer, Dordrecht, Heidelberg, New York, London, 2014), p. 169 – 191.
4. T. Takabatake, K. Suekuni, T. Nakayama, and E. Kaneshita, Phonon-Glass Electron-Crystal Thermoelectric Clathrates: Experiments and Theory, *Rev. Mod. Physics* 86, 669 – 716 (2014).
5. H. Kawaji, H. Horie, S. Yamanaka, and M. Ishikawa, Superconductivity in the Silicon Clathrate Compound $(Na, Ba)_xSi_{46,}$ *Phys. Rev. Lett*. 74, 1427 – 1429 (1995).
6. S. Yamanaka, E. Enishi, H. Fukuoka, and M. Yasukawa, High-Pressure Synthesis of a New Silicon Clathrate Superconductor, $Ba_8Si_{46}$, *Inorg. Chem*. 39, 56 – 58 (2000).
7. Slack, G. New Materials and Performance Limits for Thermoelectric Cooling in *CRC Handbook of Thermoelectrics, ed. D. M. Rowe* (CRC Press, Boca Raton, 1995), 407 – 440.
8. L. Zhang, A. Grytsiv, M. Kerber, P. Rogl, E. Bauer, and M. Zehebauer, Thermoelectric Performance of Mischmetal Skutterudites $Mm_yFe_{4-x}Co_xSb_{12}$ at Elevated Temperatures, *J. Alloys Compd.* 490, 19 – 25(2010).
9. M. Christensen, A.B. Abrahamsen, N.B. Christensen, F. Juranyi, N.H. Andersen, K. Lefmann, J. Andreasson, C.R.H. Bahl, and B.B. Iversen, Avoided Crossing of Rattler Modes in Thermoelectric Materials, *Nat. Mater*. 7, 811 – 815 (2008).
10. H. Euchner, S. Pailhès, L.T.K. Nguyen, W. Assmus, F. Ritter, A. Haghighirad, Yu. Grin, S. Paschen, and M. de Boissieu, Phononic Filter Effect of Rattling Phonons in the Thermoelectric Clathrate $Ba_8Ge_{40+x}Ni_{6-x}$ ,*Phys. Rev. B* 86, 224303 (2012).
11. S. Pailhès, H. Euchner, V.M. Giordano, R. Debord, A. Assy, S. Gomès, A. Bosak, D. Machon, S. Paschen, M.de Boissieu, Localization of Propagative Phonons in a Perfectly Crystalline Solid.

*Phys. Rev. Lett*. 113, 025506 (2014)**.**

12. T. Tadano, Y. Gohda, and S. Tsuneyuki, Impact of Rattlers on Thermal Conductivity of a Thermoelectric Clathrate: A First-Principles Study, *Phys. Rev. Lett*. 114, 095501 (2015).
13. M.M. Koza, A. Leithe-Jasper, H. Rosner, W. Schnelle, H. Mutka, M.R. Johnson, M. Krisch, L. Capogna, and Yu. Grin, Vibrational Dynamics of the Filled Skutterudites $M_{1-x}Fe_4Sb_{12}$ (M = *Ca*, *Sr*, *Ba*, and *Yb*): Temperature Response, Dispersion Relation, and Material Properties, *Phys. Rev. B* 84, 014306 (2011).
14. A. Saramat, G. Svensson, A.E.C. Palmqvist, C. Stiewe, E. Mueller, D. Platzek, S.G.K. Williams, D.M. Rowe, J.D. Bryan, and G.D. Stucky, Large Thermoelectric Figure of Merit at High Temperature in Czochralski-Grown Clathrate $Ba_8Ga_{16}Ge_{30,}$ *J. Appl. Phys*. 99, 023708 (2006).
15. X. Shi, J. Yang, S. Bai, J. Yang, H. Wang, V. Chi, J.R. Salvador, W. Zhang, L. Chen, and W. Wong-Ng,, On the Design of High-Efficiency Thermoelectric Clathrates through a Systematic Cross-Substitution of Framework Elements, *Adv. Funct. Mater*. 20, 755 – 763 (2010).
16. H. Zhang, H. Borrmann, N. Oeschler, C. Candolfi, W. Schnelle, M. Schmidt, U. Burkhardt, M. Baitinger, J.-T. Zhao, and Yu. Grin, Atomic Interactions in the *p*-Type Clathrate I $Ba_8Au_{5.3}Ge_{40.7}$, *Inorg. Chem*. 50, 1250 – 1257 (2011).
17. G.Cordier, P.Woll, Neue ternäre intermetallische Verbindungen mit Clathratstruktur: $Ba_8(T, Si)_6Si_{40}$ und $Ba_6(T, Ge)_6Ge_{40}$ mit T ≡ *Ni*, *Pd*, *Pt*, *Cu*, *Ag*, *Au*, *J. Less-Common Met*., 169, 291-302 (1991).
18. U. Aydemir, C. Candolfi, A. Ormeci, M. Baitinger, N. Oeschler, F. Steglich, and Yu. Grin, High Temperature Thermoelectric Properties of the Type-I Clathrate $Ba_8Ni_xGe_{46-x-y}\Upsilon_y$, *J. Phys. Cond. Mat*. 26, 485801 (2014).
19. U. Aydemir, C. Candolfi, A. Ormeci, M. Baitinger, U. Burkhardt, N. Oeschler, F. Steglich, and Yu. Grin, Electronic Band Structure and Low-Temperature Transport Properties of the Type-I Clathrate $Ba_8Ni_xGe_{46-x-y}\Upsilon_y$, *Dalton Trans*. 44, 7524 – 7537 (2015).
20. Y. Li, Y. Liu, N. Chen, G. Cao, Z. Feng, and J. H. Ross Jr., Vacancy and Copper-Doping Effect on Superconductivity for Clathrate Materials, *Phys. Lett*. A345, 398 – 408 (2005).
21. H. Zhang, J.-T.Zhao, M.-B.Tang, Z.-Y.Man, H.-H.Chen, and X.-X. Yang, Structure and Low Temperature Physical Properties of $Ba_8Cu_6Ge_{40}$, *J. Alloys Compd*. 476, 1 – 4 (2009).
22. N. Melnychenko-Koblyuk, A. Grytsiv, P. Rogl, H. Schmid, and G. Giester, The Clathrate $Ba_8Cu_xGe_{46-x-y}\Upsilon_y$: Phase Equilibria and Crystal Structure, *J. Solid State Chem*. 182, 1754 – 1760 (2009).
23. N. Melnychenko-Koblyuk, A. Grytsiv, L. Fornasari, H. Kaldarar, H. Michor, F. Rohrbacher, M. Koza, E. Royanian, E. Bauer, P. Rogl, M. Rotter, H. Schmid, F. Marabelli, A. Devishvili, M. Doerr, and G. Giester, Ternary Clathrates *Ba – Zn – Ge*: Phase Equilibria, Crystal Chemistry and Physical Properties, *J. Phys. Cond. Mat.* 19, 216223 (2007).
24. E. Alleno, G. Maillet, O. Rouleau, E. Leroy, C. Godart, W. Carrillo-Cabrera, P. Simon, and Yu. Grin, Germanium Vacancies and Charge Transport Properties in $Ba_8Zn_xGe_{46-x-y}\Upsilon_{y,}$ *Chem. Mater*. 21, 1485 – 1493 (2009).
25. T. Eto, K. Kishimoto, K. Koga, K. Akai, T. Koyanagi, H. Anno, T. Tanaka, H. Kurisu, S. Yamamoto, and M. Matsuura, Study of Zn-Substituted Germanium Clathrates as High Performance Thermoelectric Materials Assisted by First-Principles Electronic Structure Calculation, *Mat. Trans*. 50, 631 – 639 (2009).
26. N.A. Borshch, N.S. Pereslavtseva, and S.I. Kurganskii, Electronic Structure of Zn-substituted Germanium Clathrates, *Semiconductors* 43, 563 – 567 (2009).

27. B.Kuhl, A. Czybulka, H.-U. Schuster, Neue ternäre Käfigverbindungen aus den Systemen Barium–Indium/Zink/Cadmium–Germanium: Zintl-Verbindungen mit Phasenbreite? *Z. Anorg. Allg. Chem.* 621, 1 – 6 (1995).
28. M. Falmbigl, F. Kneidinger, M. Chen, A. Grytsiv, H. Michor, E. Royanian, E. Bauer, H. Effenberger, R. Podloucky, and P. Rogl, Cage-Forming Compounds in the *Ba – Rh – Ge* System: From Thermoelectrics to Superconductivity, *Inorg. Chem*. 52, 931 – 943 (2013).
29. N. Melnychenko-Koblyuk, A. Grytsiv, P. Rogl, M. Rotter, E. Bauer, G. Durand, H. Kaldarar, R. Lackner, H. Michor, E. Royanian, M. Koza, and G. Giester, Clathrate Formation in the *Ba – Pd – Ge* System: Phase Equilibria, Crystal Structure, and Physical Properties, *Phys. Rev*. B76, 144118 (2007).
30. I. Zeiringer, M.X. Chen, I. Bednar, E. Royanian, E. Bauer, R. Podloucky, A. Grytsiv, P. Rogl, H. Effenberger, Phase Equilibria, Crystal Chemistry, Electronic Structure and Physical Properties of *Ag – Ba – Ge* Clathrates, *Acta Mater*. 59, 2368 – 2384 (2011).
31. N. Melnychenko-Koblyuk, A. Grytsiv, S. Berger, H. Kaldarar, H. Michor, F.Rohrbacher, E. Royanian, E. Bauer, P. Rogl, H. Schmid, and G. Giester, Ternary Clathrates *Ba – Cd – Ge*: Phase Equilibria, Crystal Chemistry and Physical Properties, *J. Phys. Cond. Mat*. 19, 046203 (2007).
32. N.A.Borshch, N.S.Pereslavtseva, S.I.Kurganskii, Electron Structure and Spectral Characteristics of Cd-substituted Ge-based Clathrates, *Semiconductors* 44, 987 – 992 (2010).
33. M. Falmbigl, A. Grytsiv, P. Rogl, and G. Giester, Clathrate Formation in the Systems *Ba – Ir* – e and *Ba* – {*Rh*, *Ir*} – *Si*: Crystal Chemistry and Phase Relations, *Intermetallics* 36, 61 – 72 (2013).
34. N. Melnychenko-Koblyuk, A. Grytsiv, P. Rogl, M. Rotter, R. Lackner, E. Bauer, L. Fornasari, F.Marabelli, and G. Giester, Structure and Physical Properties of Type-I Clathrate Solid-Solution $Ba_8Pt_xGe_{46-x-y}\Upsilon_y$ ($\Upsilon$=vacancy), *Phys.Rev.B* 76, 195124 (2007).
35. I. Zeiringer, N. Melnychenko-Koblyuk, A. Grytsiv, E. Bauer, G. Giester, and P. Rogl, *Phase* Equilibria, Crystal Chemistry and Physical Properties of Au-Ba-Ge Clathrates, *J. Phase Eq. Diff*. 32, 115 – 127 (2011).
36. S.Y. Rodriguez, L. Saribaev, J.H. Ross Jr., Zintl Behavior and Vacancy Formation in Type-I *Ba – Al – Ge* Clathrates, *Phys. Rev. B* 82, 064111 (2010).
37. N.L. Okamoto, K. Kishida, K. Tanaka, and H. Inui, Crystal Structure and Thermoelectric Properties of Type-I Clathrate Compounds in the *Ba – Ga – Ge* System, *J. Appl. Phys*. 100, 073504 (2006).
38. W. Carrillo-Cabrera, R. Cardoso Gil, S. Paschen, and Yu. Grin, Crystal Structure of $Ba_8Ga_{4.44}Ge_{39.14}\Upsilon_{2.42}$, $Ba_8Ga_{8.62}Ge_{36}\Upsilon_{1.38}$, and $Ba_8Ga_{12.35}Ge_{33.27}\Upsilon_{0.38}$, Three Clathrate-I Variants, *Z. Kristallog. NCS* 217, 183 – 185 (2002).
39. W. Carrillo-Cabrera, S. Budnyk, Y. Prots, and Yu. Grin, $Ba_8Ge_{43}$ Revisited: a 2a'×2a'×2a' Superstructure of the Clathrate-I Type with Full Vacancy Ordering, *Z. Anorg. Allg. Chem*. 630, 2267 – 2276 (2004).
40. U. Aydemir, C. Candolfi, H. Borrmann, M. Baitinger, A. Ormeci, W. Carrillo-Cabrera, C.Chubilleau, B. Lenoir, A. Dauscher, N. Oeschler, F. Steglich,, and Yu. Grin, Crystal Structure and Transport Properties of $Ba_8Ge_{43}\Upsilon_3$ , *Dalton Trans*. 39, 1078 – 1088 (2010).
41. Yu. Grin, A. Savin, and B. Silvi, *The ELF Perspective of Chemical Bonding*. in *The Chemical Bond: Chemical Bonding Across the Periodic Table*, eds. G. Frenking, S. Shaik, Wiley-VCH, 2014, p. 1 – 53.
42. M. Kohout, A. Measure of Electron Localizability, *Int. J. Quantum Chem*. 97, 651 – 658 (2004).
43. Kohout, M., Wagner, F. R., Grin, Yu. *Electron localization function for transition-metal compounds*. Theor. Chem. Acc. 108, 2002, 150 – 156.

44. R.F.W. Bader, *Atoms in Molecules, A Quantum Theory* (Clarendon Press, Oxford, 1995).
45. S. Raub, G. Jansen, A Quantitative Measure of Bond Polarity from the Electron Localization Function and the Theory of Atoms in Molecules, *Theor. Chem. Acc*. 106, 223 – 232 (2001).
46. A.Ormeci, Yu. Grin, Chemical Bonding in $Al_5Co_2$: The Electron Localizability - Electron Density Approach, *Isr. J. Chem*. 51, 1349 – 1354 (2011).
47. D. Bende, Yu. Grin, and F.R. Wagner, Covalence and Ionicity in *MgAgAs*-Type Compounds, *Chem. Eur. J*. 20, 9702 – 9708 (2014).
48. D. Bende, F.R. Wagner, and Yu. Grin, 8-N Rule and Chemical Bonding in Main-Group *MgAgAs*-type Compounds, *Inorg. Chem*. 54, 3970 – 3978 (2015).
49. F.R. Wagner, V. Bezugly, M. Kohout, and Yu. Grin, Charge Decomposition Analysis of the Electron Localizability Indicator: A Bridge between the Orbital and Direct Space Representation of the Chemical Bond, *Chem. Eur. J*. 13, 5724 – 5741 (2007).
50. K. Koepernik, H. Eschrig, Full-Potential Nonorthogonal Local-Orbital Minimum-Basis Band-Structure Scheme, *Phys. Rev. B*59, 743 – 1757 (1999).
51. J.P. Perdew, Y. Wang, Accurate and Simple Analytic Representation of the Electron-Gas Correlation Energy, *Phys. Rev. B* 45, 13244 – 13249 (1992).
52. J.P. Perdew, K. Burke, and M. Ernzerhof, Generalized Gradient Approximation Made Simple, *Phys. Rev. Lett*. 77, 3865 – 3868 (1996).
53. M. Kohout, F.R. Wagner, and Yu. Grin, Atomic Shells From the Electron Localizability in Momentum Space, *Int. J. Quantum Chem*. 106, 1499 – 1507 (2006).
54. M. Kohout, Bonding Indicators from Electron Pair Density Functionals, *Faraday Discuss.* 135, 43 – 54 (2007).
55. A. Ormeci, H. Rosner, F.R. Wagner, M. Kohout, and Yu. Grin, Electron Localization Function in Full-Potential Representation for Crystalline Materials, *J. Phys. Chem*. A110, 1100 – 1105 (2006).
56.M. Kohout, *Program DGRID, version 4.6*, Radebeul, Germany, 2011.
57. J. Zhao, A.Buldum, J.P.Lu, Structural and Electronic Properties of Germanium Clathrates $Ge_{46}$ and $K_8Ge_{46,}$, *Phys. Rev. B* 60, 14177 (1999).
58. C. Candolfi, A. Ormeci, U. Aydemir, M. Baitinger, N. Oeschler, Yu. Grin, and F. Steglich, Multiband Conduction in the Type-I Clathrate $Ba_8Ge_{43}\Upsilon_3$ , *Phys. Rev. B* 84, 205118 (2011).
59. C. Candolfi, U. Aydemir, A. Ormeci, M. Baitinger, N. Oeschler, F. Steglich, and Yu. Grin, Low-Temperature Magnetic, Galvanomagnetic, and Thermoelectric Properties of the Type-I Clathrates $Ba_8Ni_xSi_{46-x}$ , *Phys. Rev. B* 83, 205102 (2011).
60. W. Jung,, H. Kessens, A. Ormeci, W. Schnelle, U. Burkhardt, H. Borrmann, H.D. Nguyen, M.Baitinger, and Yu. Grin, Synthesis,Crystal Structure and Physical Properties of the Clathrate-I Phase $Ba_8Rh_xSi_{46-x-y}\Upsilon_y$ , *Dalton Trans*. 41, 13960 – 13968 (2012).
61. U. Aydemir, C. Candolfi, A. Ormeci, Y. Oztan, M.Baitinger, N. Oeschler, F. Steglich, and Yu. Grin, Low-Temperature Thermoelectric, Galvanomagnetic, and Thermodynamic Properties of the Type-I Clathrate $Ba_8Au_xSi_{46-x}$, *Phys. Rev. B* 84, 195137 (2011).
62. P. Tomeš, M. Ikeda, A. Sidorenko, S. Paschen, C. Candolfi, M. Baitinger, H.D. Nguyen, L. D.K.Nguyen, and Yu. Grin, Structural and physical properties of the clathrate-I phase $Ba_8Ir_xGe_{46-x-y}\ \Upsilon_y$ (x<0.4). 2016, submitted.
63. U. Aydemir, C. Candolfi, A. Ormeci, H. Borrmann, U. Burkhardt, Y. Oztan, N. Oeschler, M.Baitinger, F. Steglich, and Yu. Grin, Synthesis, Crystal Structure, and Physical Properties of the Type-I Clathrate $Ba_{8-\delta}Ni_x\Upsilon_ySi_{46-x-y}$, *Inorg. Chem*. 51, 4730 – 4741 (2012).

64. M. Baitinger, B. Boehme, A. Ormeci, and Yu. Grin, Solid State Chemistry of Clathrate Phases: Crystal Structure, Chemical Bonding and Preparation Routes. In: *The Physics and Chemistry of Inorganic Clathrates*, ed. G. S. Nolas (Springer, Dordrecht, Heidelberg, New York, London, 2014), pp. 35 – 64.
65. H.D. Nguyen, I. Antonyshyn, K. Meier-Kirchner, I. Veremchuk, W. Schnelle, U.Burkhardt, R. Carodoso Gil, B. Böhme, M. Baitinger, and Yu. Grin, Thermoelectric Characterization of the p-type Clathrate-I $Ba_8Au_{5.2+x}Ge_{40.8-x-y}\Upsilon_y$, 2016, submitted.
66. A. Ormeci, A. Simon, and Yu. Grin, *Structural Topology and Chemical Bonding in Laves Phases*, *Angew. Chem. Int. Ed.* 49, 8997 – 9001 (2010).
67. H. Zhang, M. Baitinger, L. Fang, W. Schnelle, H. Borrmann, U. Burkhardt, A. Ormeci, J.-T. Zhao, and Yu. Grin, Synthesis and Properties of Type-I Clathrate Phases $Rb_{8-x-t}K_x\Upsilon_tAu_yGe_{46-y}$. *Inorg. Chem.* 52, 9720 – 9726 (2013).
68. X. Yan, E. Bauer, P. Rogl, and S. Paschen, Structural and Thermoelectric Properties of $Ba_8Cu_5Si_xGe_{41-x}$ Clathrates, *Phys. Rev. B* 87, 115206 (2013).

Submitted 08.01.2016